

ENDORSEMENT

I, Nabila Binti Mustapa hereby declare that all corrections and comments made by the supervisor and examiner have been taken consideration and rectified accordingly.

(Signature of Student)

Date:

(Signature of Supervisor)

Name:

Date:

(Signature of Examiner)

Name:

Date:

DECLARATION

This thesis is the result of my own investigation, except where otherwise stated and has not previously been accepted in substance for any degree and is not being concurrently submitted in candidature for any other degree.

(Signature of Student)

Date:

ACKNOWLEDGMENT

In performing this project, many help and guidance had been received from some respected person, who deserve greatest gratitude. Without the participation and assistance of these people, the project could not have been possible.

First and foremost, I would like to thank to my supervisor, Assoc. Prof. Dr Farzad Ismail whose expertise, generous guidance and support that made it possible for me to work and complete the whole project within the period of time. Every step and improvement in analysis and simulation for this project had been done with the aid of Dr Farzad.

Special gratitude to the staff members of School of Aerospace Engineering, Mrs Rahayu, Dr. Chang Wei Shyang and Dr Hafiz Hafifi for their help in delivering a useful information to the project. I would definitely not be able to do it on my own. Sincere thanks to Zularieff Redzwan bin Sulaiman and Chan Quan Xin who rendered their help during the period of the project regarding on the simulation problem.

Finally, greatest appreciation to my parents, all relatives, friends, seniors and my pet who in one way or another shared their encouragement and support, either morally, financially and physically.

Above all, to the Great Almighty, the author of knowledge and wisdom.

STUDY OF AERODYNAMICS PERFORMANCE OF GLIDERS USING COMPUTATIONAL FLUID DYNAMICS ANALYSIS

ABSTRACT

Developments in geometry modelling, surface and volume grid generation and flow simulation algorithms provide a route to accurate flow field predictions for increasingly complex and realistic format. Hence, computational aerodynamics has appeared as a crucial enabling technology for the design and development of flight vehicles (Slater, 2008). A glider named as UCC-14 is selected to be computationally analysed on their aerodynamics performance specifically lift and drag coefficients. The models are varied in terms of types of airfoil and wing planform which include straight with dihedral tip, elliptical and tapered with dihedral tip.

A hand-launched glider is a free flight aircraft that is supported in flight by the dynamic reaction of the air against its lifting surface and not depending on engine. The thrust is fully depended on the force generated by the launcher. Aircraft wings are the lifting surfaces with a specific airfoil sections (Haque et al., 2015). The performance of an aircraft as well as the efficiency mostly depends on the aerodynamic characteristics lift, drag, lift to drag ratio of wings. The effects of wing shapes are very crucial to the aircraft aerodynamic performance (Haque et al., 2015) in terms of the lift and drag distributions along the wing span. The aerodynamic properties of a glider aircraft depend on their shape, imposing significant design constraints (Fukusato et al., 2018). One of the important design phases of an aerodynamically efficient wing is the selection of an appropriate airfoil. The airfoil

selection of a wing design firstly requires performing aerodynamic performance analyses of different airfoils for the purpose of the design (Fukusato et al., 2018).

Conventional hand-launched gliders commonly fly at low altitude and low velocity. In this project, the flow is assumed to be laminar at steady state (gliding phase) with incompressible flow. Since the gliding altitude does not exceed 10 meters, the boundary condition which includes inlet and outlet pressure, temperature, and density can be assumed to be the same as at sea-level. A Reynolds number range of 60,400 is specified as the flow properties based on the reference from the journal “Summary of Low-Speed Airfoil Data”.

The gliders dimensions are measured manually and drawn into a computer-aided-drawing CAD software (CATIA V5) as a 3 dimensional geometry. A 2-dimensional analysis is done on RG-14, AG-37 and MH-32 airfoil. All models are simulated and computationally analysed. Comparison of the results on lift and drag coefficient of the models are made to differentiate the aerodynamic effectiveness of each design. The computational results will be compared with the wind tunnel experiment data to obtain the validation of the simulation.

PENGAJIAN TENTANG PRESTASI AERODINAMIK PESAWAT GLIDERS MENGUNAKAN ANALISIS PENGKOMPUTERAN DINAMIK CECAIR

ABSTRAK

Perkembangan pemodelan geometri, permukaan dan isi padu grid dan algoritma simulasi aliran menyediakan laluan ke ramalan medan aliran yang tepat untuk format yang semakin rumit dan realistik. Oleh itu, aerodinamik pengkomputeran telah muncul sebagai teknologi yang penting bagi reka bentuk dan pembangunan kenderaan penerbangan (Slater, 2008). Pesawat luncur yang dinamakan sebagai UCC-14 dipilih untuk dianalisa secara analitikal atas prestasi aerodinamik mereka khususnya pekali angkat dan pekali heret. Model-model ini bervariasi dari segi jenis aerofoil dan bentuk pelan sayap yang termasuk lurus dengan struktur dihedral di hujung.

Sebuah pesawat luncur yang dilancarkan menggunakan tangan ialah pesawat yang disokong dalam penerbangan oleh reaksi dinamik udara terhadap permukaan mengangkat dan tidak bergantung kepada enjin. Tujah sepenuhnya bergantung kepada daya yang dihasilkan oleh pelancar itu. Sayap pesawat adalah permukaan mengangkat dengan keratan rentas 'airfoil' tertentu (Haque et al., 2015). Prestasi serta kecekapan pesawat bergantung terutamanya pada ciri-ciri aerodinamik iaitu daya mengangkat, daya menyeret, nisbah daya mengangkat kepada daya menyeret sayap. Bentuk sayap memberi impak yang sangat penting untuk prestasi aerodinamik pesawat (Haque et al., 2015) dari segi pembahagian daya mengangkat dan menyeret sepanjang bidang sayap. Ciri-ciri aerodinamik pesawat luncur bergantung kepada bentuknya, mengenakan kekangan reka bentuk yang ketara (Fukusato et al., 2018). Salah satu fasa penting dalam mereka bentuk sayap adalah pemilihan keratan

rentas 'airfoil' yang sesuai. Pemilihan 'airfoil' terlebih dahulu memerlukan analisis prestasi aerodinamik jenis 'airfoil' yang berbeza untuk tujuan reka bentuk (Fukusato et al., 2018).

Pesawat luncur konvensional biasanya terbang pada ketinggian dan halaju yang rendah. Dalam projek ini, aliran tersebut dianggap sebagai laminar pada keadaan stabil (fasa meluncur) dengan aliran yang tidak boleh dimampatkan. Oleh kerana ketinggian meluncur tidak melebihi 10 meter, keadaan sempadan termasuk tekanan masuk dan keluar, suhu, dan ketumpatan boleh diandaikan sama dengan paras laut. Julat nombor Reynolds sebanyak 60,400 telah ditetapkan sebagai sifat aliran berdasarkan rujukan daripada jurnal "Summary of Low-Speed Airfoil Data".

Dimensi pesawat luncur diukur secara manual dan dilukis ke dalam perisian lukisan-dibantu-komputer (CATIAV5) sebagai geometri 3 dimensi. Analisis 2 dimensi dilakukan pada 3 jenis 'airfoil' iaitu RG-14, AG-37 dan MH-32. Semua model disimulasikan dan dianalisis secara analitikal. Perbandingan hasil pada pekali angkat dan seretan model dibuat untuk membezakan keberkesanan aerodinamik setiap reka bentuk. Keputusan komputasi akan dibandingkan dengan hasil daripada ujian terowong angin untuk mendapatkan pengesahan simulasi.

TABLE OF CONTENTS

ENDORSEMENT	I
DECLARATION	II
ACKNOWLEDGMENT	III
ABSTRACT	IV
ABSTRAK	VI
LIST OF FIGURES	X
LIST OF TABLES	XII
LIST OF ABBREVIATIONS	XIII
LIST OF SYMBOLS	XIV
CHAPTER 1	1
1.1 Background	. 1
1.2 Problem Statement	2
1.3 Objectives of Research	. 2
CHAPTER 2	3
2.1 Introduction	3
2.2 Structure of an Airfoil	. 3
2.3 Aerodynamic Forces Acting on a Body	. 4
2.4 Laminar Flow	6
2.5 Flow Separation	7
2.6 Structured and Unstructured Mesh	8
CHAPTER 3	12
3.1 Introduction	12
3.2 Modeling of Geometry	12
3.3 Grid Generation	. 13
3.4 Simulation Setup 2-Dimension	16

3.5	Simulation Setup for 3-Dimension	18
CHAPTER 4		20
4.1	Introduction	20
4.2	Grid Independence Test	20
4.3	Result Validations	22
4.4	Aerodynamic Performance of Airfoil	26
4.5	Simulation of 3-Dimensional Fluid Flow	37
CHAPTER 5		41
5.1	Introduction	41
5.2	Conclusion	41
5.3	Future Works and Recommendation.	42
REFERENCES		43
APPENDIX		45

LIST OF FIGURES

Figure 2.1: Basic terminology of an airfoil.	3
Figure 2.2: Symmetrical airfoil and Cambered airfoil.	4
Figure 2.3: Resultant aerodynamic force and its components acting on a wing section.	5
Figure 2.4: Diagram of laminar boundary layer over an airfoil went to turbulent after the increase of angle of attack.	6
Figure 2.5: Stages of boundary layer development on a flat plate subjected to an adverse pressure gradient. Arrows show flow direction, with length indicating velocity and mean flow velocity emboldened, boundary layer in blue and zone of vortex formation or 'wake' in red.	8
Figure 2.6: Nodal indexing of elemental cells in two and three dimensions for a structured mesh.	9
Figure 2.7: A structured and an unstructured mesh for a circular cylinder	10
Figure 3.1: The geometry of UCC-14.	13
Figure 3.2: The t-type meshing with 4 faces	14
Figure 3.3: Meshing focusing near the airfoil area	14
Figure 3.4: Grid generation for 3D glider in fluid domain	15
Figure 3.5: Meshing focusing on the inflation	15
Figure 4.1: Comparison of different grids used in ANSYS with the experimental value of lift coefficient C_l .	21
Figure 4.2: Comparison of different grids used in ANSYS with the experimental value of drag coefficient C_d .	21

Figure 4.3: Residual plot showing the convergence of the solution.	23
Figure 4.4: Graph of lift coefficient against the angle of attack for RG14 airfoil with experimental and computational data.	23
Figure 4.5: Graph of drag coefficient against the angle of attack for RG14 airfoil with experimental and computational data.	24
Figure 4.6: Sample pattern of diffusive, undershoot and overshoot solution.	25
Figure 4.7: Graph of computational lift coefficient against angle of attack for RG14, AG37 and MH32.	27
Figure 4.8: Graph of computational drag coefficient against angle of attack for RG14, AG37 and MH32.	28
Figure 4.9: Airfoil with blunt trailing edge produce larger vortex shading.	29
Figure 4.10: Airfoil with sharp trailing edge with smaller vertex shading.	29
Figure 4.11: The residual plot of the simulation of fluid flow across UCC-14.	37
Figure 4.12: The velocity contour plot at the symmetry surface across UCC-14.	38
Figure 4.13: The streamline of velocity across the glider presenting the dominance of laminar flow.	39
Figure 4.14: The pressure contour plot at the symmetry surface across UCC-14.	39
Figure 4.15: The pressure contour plot focusing at the lower surface of horizontal stabilizer.	40

LIST OF TABLES

Table 3.1: Input Parameter for the simulation setup of 2D.	16
Table 3.2: Under relaxation factor for 2D analysis.	17
Table 3.3: Input Parameter for the simulation setup of 3D.	18
Table 3.4: Under relaxation factor for 2D analysis.	18
Table 4.1: Velocity contour plot for RG14, AG37 and MH32 airfoil for AOA= -3.23°.	30
Table 4.2: Velocity contour plot for RG14, AG37 and MH32 airfoil for AOA= 0.93°.	31
Table 4.3: Velocity contour plot for RG14, AG37 and MH32 airfoil for AOA= 5.09°.	32
Table 4.4: Pressure contour plot for RG14, AG37 and MH32 airfoil for AOA= -3.23°.	34
Table 4.5: Pressure contour plot for RG14, AG37 and MH32 airfoil for AOA= 0.93°.	35
Table 4.6: Pressure contour plot for RG14, AG37 and MH32 airfoil for AOA= 5.09°.	36

LIST OF ABBREVIATIONS

AOA Angle of Attack

LIST OF SYMBOLS

C_L	Lift coefficient
C_D	Drag coefficient

CHAPTER 1

INTRODUCTION

1.1 Background

A hand-launched glider is a free flight aircraft that is supported in flight by the dynamic reaction of the air against its lifting surface and not depending on engine. The thrust is fully depending on the force generated by the launcher. Aircraft wings are the lifting surfaces with a specific airfoil sections (Haque et al., 2015). The performance of an aircraft as well as the efficiency mostly depends on the aerodynamic characteristics lift, drag, lift to drag ratio of wings. The effects of wing shape are is very crucial to aircraft aerodynamic performance (Haque et al., 2015).

Recent advances of computer hardware and computer simulation techniques have enabled us to solve the Euler/Navier-Stokes equations for flow around fully precise and complex models. Although a traditional approach using structured mesh is suitable for computation of high-Reynolds number viscous flows, it takes much time to deal with a complex geometry. On the other hand, an approach using unstructured mesh has a capability of easy mesh generation for a complex configuration. A hybrid mesh composed of tetrahedrons, prisms and pyramids enable accurate computations for high-Reynolds number flows with thin boundary layers developed along the wall. The drawback of the unstructured mesh, however, is its excessive overheads in memory and CPU time as compared with those in structured meshes (Fujita et al., 2003) .

Navier-Stokes solvers for complete aircraft configurations have been used for a number of years. Geometric complexities are tackled through the use of either unstructured or block structured meshes. For multi-disciplinary work such as shape optimisations, where repetitive calculations on the same or similar mesh are required, the efficiency of the flow solver is more important than the cost of generating the mesh. This makes the use of block structured grids viable. (Woodgate et al., 2000).

1.2 Problem Statement

The study of aerodynamics of hand launched glider are hardly seen. The aerodynamic properties of a glider aircraft depends on their shape, imposing significant design constraints (Fukusato et al., 2018). One of the important design phases of an aerodynamically efficient wing is selection of the appropriate airfoil. Airfoil selection of a wing design firstly requires performing aerodynamic performance analyses of different airfoils to compare according to the purpose of the design (Fukusato et al., 2018). The whole research also significantly establishing skills on carrying out Computational Fluid Dynamic analysis.

1.3 Objectives of Research

The objectives of this research are:

- 1.3.1 To study the aerodynamic of RG 14 airfoil, MH 32 airfoil and AG 37 airfoil.
- 1.3.2 To study three-dimensional fluid dynamic simulation on glider.
- 1.3.3 To compare the wind tunnel test data with the computational fluid dynamic analysis.

CHAPTER 2

LITERATURE REVIEW

2.1 Introduction

This chapter reviews literature regarding aerodynamic characteristic of airfoil, flow in low Reynold's number, flow separation and meshing type and properties for computational fluid dynamics (CFD).

2.2 Structure of an Airfoil

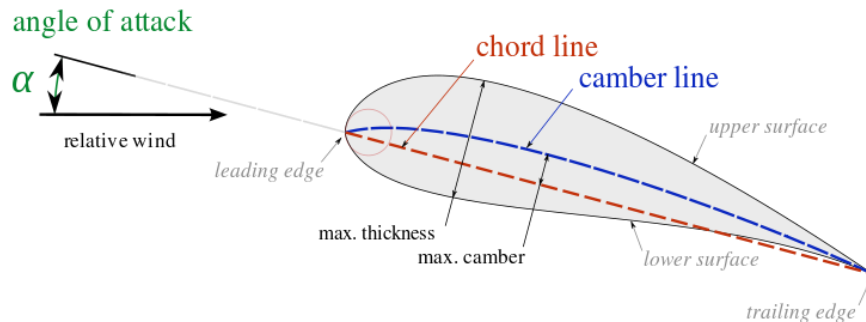


Figure 2.1: Basic terminology of an airfoil.
(Source: Olivier Cleynen 19, April 2011)

Typical airfoil can be divided into four sections which are the leading edge, trailing edge, upper surface or suction side, and lower surface. The components of airfoils has been elaborated by (Mamadaminov, 2013). The line connecting leading edge with trailing edge is called the chord line. The curve that passes through mid-point of the upper surface and the lower surface of an airfoil is called mean camber line. The typical airfoil structure is shown in Figure 1. The thickness of an airfoil is defined the maximum distance between the upper

surface and the lower surface and it is generally provided as a fraction of the chord length. For example twelve percent thick airfoil has a maximum thickness that is twelve percent of the airfoil's chord length (Mamadaminov, 2013). There are commonly two types of airfoil, symmetrical and cambered which serves different purpose.

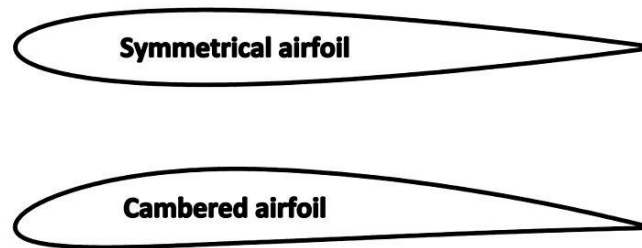


Figure 2.2: Symmetrical airfoil and Cambered airfoil.
(Source: J Doug McLean 15 May 2014)

2.3 Aerodynamic Forces Acting on a Body

A body pass through a medium of fluid eventually create lift force. The lift generated is perpendicular while drag is parallel to the horizontal streamline. The concept of generation of lift has been explained by (KHAN, 2015).

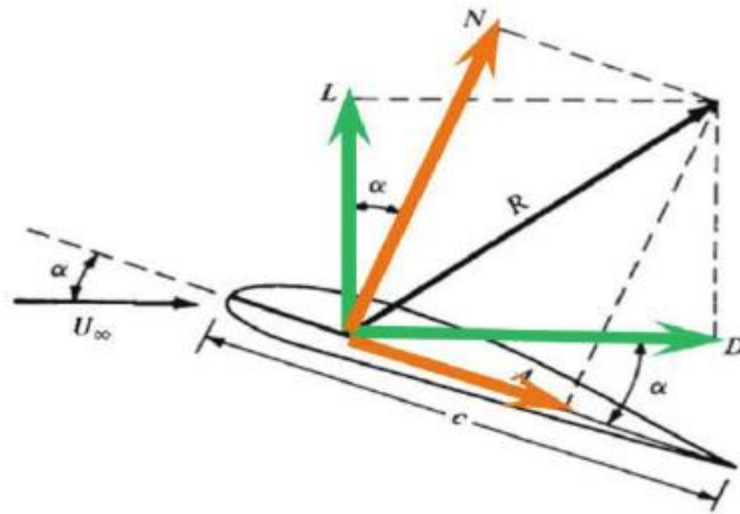


Figure 2.3: Resultant aerodynamic force and its components acting on a wing section.

Bernoulli's principle stated that at point along horizontal streamline, higher pressure regions have lower fluid speed and lower pressure regions have higher fluid speed (KHAN, 2015). According to the principle the relation of velocity and pressure is inversely proportional. Thus, the pressure at the airfoil bottom surface is higher since the velocity is slower. The upper surface will have lower pressure. This differences of the two surfaces flow pressure will eventually create lift force upward the horizontal streamline (KHAN, 2015). An integration of a pressure distribution over an airfoil chord for both upper and lower surfaces is known to provide normal and axial force acting on an airfoil section when shear stress due to viscous effect is neglected (D. Anderson and P. Hunter, 1987).

The divergence in pressure created above and below a vehicle's body as it moves through the surrounding viscous air is a measure of aerodynamic lift coefficient (Heisler, 2002).

The measure of the effectiveness of a streamline aerodynamic body shape in reducing the air resistance to the forward motion of a moving body is the representation of aerodynamic drag coefficient C_D . A streamline body is to enable to move easily through the surrounding viscous air with the minimum of resistance indicate that it has low drag coefficient C_D ; contrarily a high drag coefficient C_D is caused by poor streamlining of the body profile which causes high air resistance when the body is moving (Heisler, 2002).

2.4 Laminar Flow

The behavior of the laminar boundary layers on low-Reynolds-number airfoils significantly affects the aerodynamic performances of the airfoils. Laminar boundary layers are unable to withstand any significant adverse pressure gradient hence laminar flow separation is usually found on low-Reynolds-number airfoils. Post separation behavior of laminar boundary layers responsible for the degradation in the aerodynamic performances of low-Reynolds-number airfoils. The deterioration is exhibited by an increase in drag and decrease in lift.

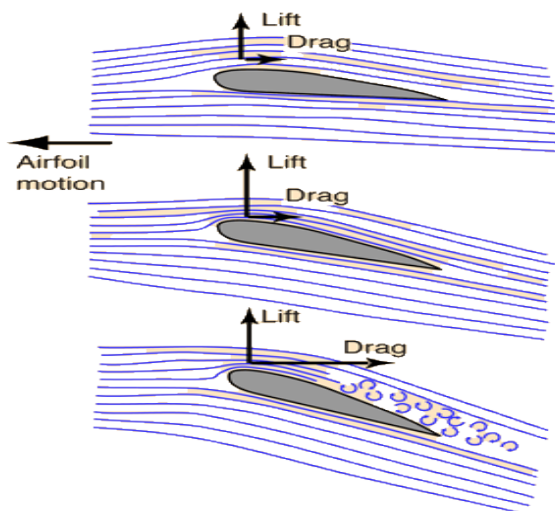


Figure 2.4: Diagram of laminar boundary layer over an airfoil went to turbulent after the increase of angle of attack.

Low speed wind tunnel tests have shown that when a laminar boundary layer separates from the leading edge of a thin airfoil at incidence the flow often becomes attached to the surface again some distance downstream. The region of separated flow is called a bubble and its chord-wise dimension may vary from a minute fraction of the chord to a length comparable with the chord, depending on incidence, Reynolds number and type of airfoil section (P. R. Owen, 1955). For more streamlined bodies, such as an aircraft wing at cruise, the overall drag is dominated by skin-friction drag and hence a laminar boundary layer is preferable (J, 1997)

2.5 Flow Separation

According to (Horton,1968) the separated laminar boundary layers would rapidly transit to turbulence, and then reattach to the airfoil surface as a turbulent boundary layer when the adverse pressure gradient over the airfoil surface is adequate (Horton, 1968). This would result in the formation of a laminar separation bubble. As the adverse pressure gradient becomes more severe with the increasing angle of attack, the separation bubble would suddenly burst, which will subsequently result in airfoil stall [semantic scholar].

The severe adverse pressure gradient that develops in the neighbourhood of the sharply curved nose is the main reason behind this occurrence. Until recently the phenomenon was not considered to have much practical aeronautical significance, since wings in common use were of such thickness (greater than 0.1 chord) that the stall usually began near the trailing edge in the form of a turbulent boundary layer separation (P. R. Owen, 1955).

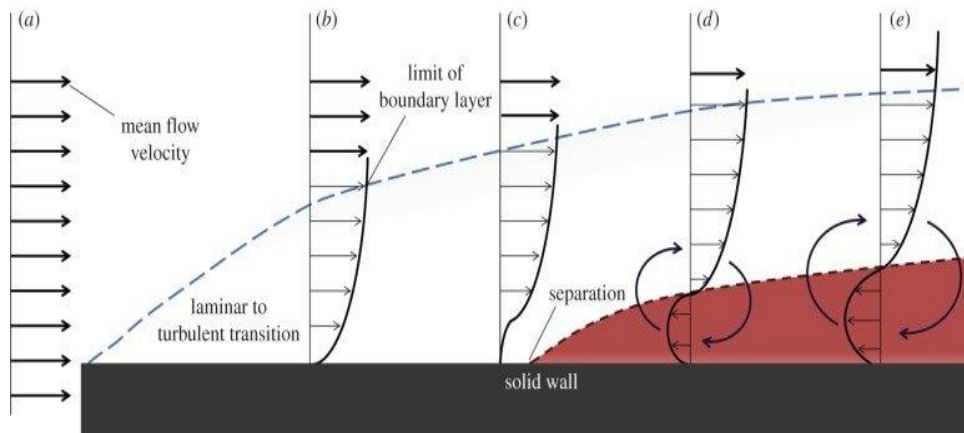


Figure 2.5: Stages of boundary layer development on a flat plate subjected to an adverse pressure gradient. Arrows show flow direction, with length indicating velocity and mean flow velocity emboldened, boundary layer in blue and zone of vortex formation or ‘wake’ in red.

(Source: Hydrodynamics of fossil fishes)

Separation occurs in response to adverse pressure gradients, usually found where a flow boundary undergoes a sharp change of direction (Allen, 1982). At a specific angle of attack this adverse pressure gradient reaches such a high value that the boundary layer instantly detaches from the leading edge (Timmer and Bak, 2013). (Gudmundsson, 2014) suggested that the trailing edge must be deliberately thickened to improve adverse pressure gradients.

2.6 Structured and Unstructured Mesh

The advantage of structured mesh is that the points of an elemental cell can be easily addressed by a double of indices (i, j) in two dimensions or a triple of indices (i, j, k) in three dimensions. The cells of an elemental face are identified by the indices and the cell edges form continuous mesh lines that begin and end on opposite elemental faces hence forming

direct connectivity as shown in Figure. The central cell is connected by four neighbouring cells in two dimension geometry while six in three dimensions geometry.

However, the increase in grid nonorthogonality or skewness will occur when structured mesh is adapted in complex geometry that can cause unphysical solutions. This is due to the transformed governing equations. Hence, the accuracy and efficiency of the numerical algorithm will be affected.

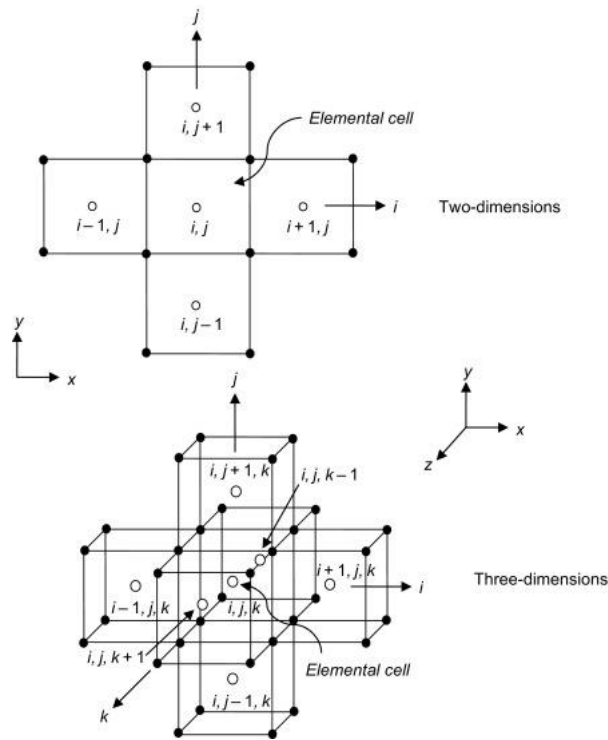


Figure 2.6: Nodal indexing of elemental cells in two and three dimensions for a structured mesh.

Unstructured meshing allow cells to be patched up freely within the computational domain. The most common shape of an *unstructured* element is a triangle for 2D or a tetrahedron 3D geometry. Having said that, quadrilateral or hexahedral shape also can be

applied. Random shape geometries especially for domains having high-curvature boundaries utilize most of unstructured mesh. Structured grid tends to produce highly skewed cells in curvature boundaries to satisfy the geometrical constraints. This type of mesh generally leads to numerical instabilities and degradation of the computational results. It will be more preferable to remesh the geometry with an *unstructured* triangular mesh.

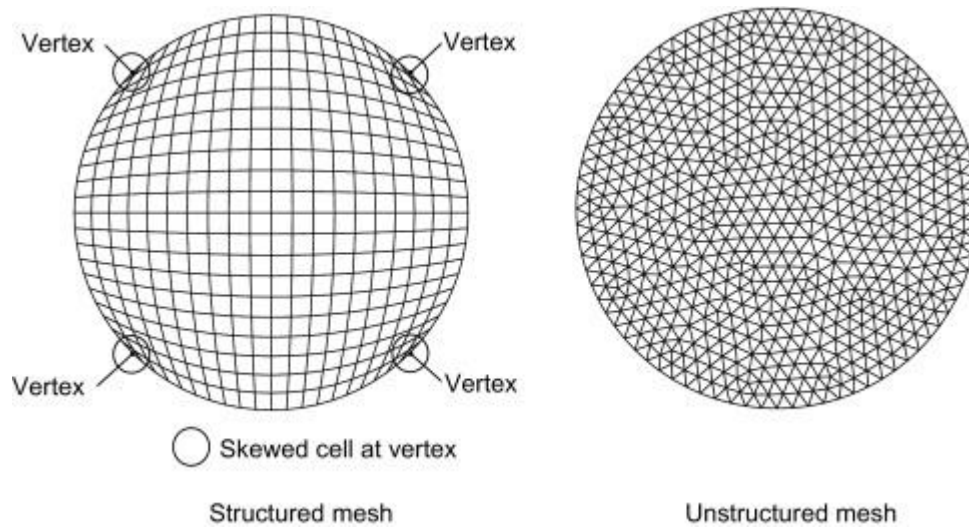


Figure 2.7: A structured and an unstructured mesh for a circular cylinder.

However, the points of an elemental cell for an *unstructured* mesh generally cannot be simply identified by a double of indices (i, j) in two dimensions or a triple of indices (i, j, k) in three dimensions. An elemental cell may have a random number of neighbouring cells attaching to it making the data treatment and connection arduously complicated. In fact, wall boundary layers is difficult to be resolved by triangular or tetrahedral cells in comparison with quadrilateral or hexahedron cells. Another disadvantage in connection with data treatment and connectivity of cells is the requirement of more complex solution

algorithms to solve the flow-field variables. This may result in increased computational times to obtain a solution thus reducing computational efficiency.

Maximum flexibility in matching mesh cells with the boundary surfaces can be achieved by applying hybrid grids that combine different element types such as triangular and quadrilateral in two dimensions or tetrahedron, hexahedron, prisms, and pyramids in three dimensions and allocating cells of various element types in other parts of the complex flow regions. Grid quality is usually improved by generating quadrilateral or hexahedron elements in resolving boundary layers near solid walls, whilst triangular or tetrahedral elements or polyhedral cells for the rest of the flow domain. This generally leads to both accurate solutions and better convergence for the numerical solution methods (Tu et al., 2018).

The solution of the Navier-Stokes equations at high Reynolds number requires grids, which are highly stretched in the shear layers. Although such grids can also be constructed from tetrahedral elements, it is advisable to use prisms or hexahedra in the viscous flow regions and tetrahedron outside. This improves not only the solution accuracy, but it also saves the number of elements, faces, and edges. Thus, the memory and run-time requirements of the simulation are reduced significantly (Blazek, 2015).

CHAPTER 3

METHODOLOGY

3.1 Introduction

In this chapter, the modeling of the 2-D geometry with the selected domain using ANSYS Design Modeler and 3-D geometry using CatiaV5 will be explained and the simulation of the geometry in ANSYS Fluent will be elaborated.

3.2 Modeling of Geometry

A two-dimensional geometry is sketched in ANSYS Design Modeler software in order to analyze the aerodynamic characteristics of the airfoil using Computational Fluid Dynamics Analysis method. The coordinate of the specific type of airfoil is obtained from an online source . The chord length of the airfoil is set as 1 meter and a dynamically similar comparison is done to obtain the correct velocity with reference Reynold's number of 60400 following the wind tunnel properties in "Summary of Low-Speed Airfoil Data".

C-domain is used for this simulation and the distance of the front boundary from the leading edge is six times the chord length while the distance of the back boundary from the trailing edge is twelve times the chord length. The upper and bottom boundaries are six times the chord length from the airfoil.

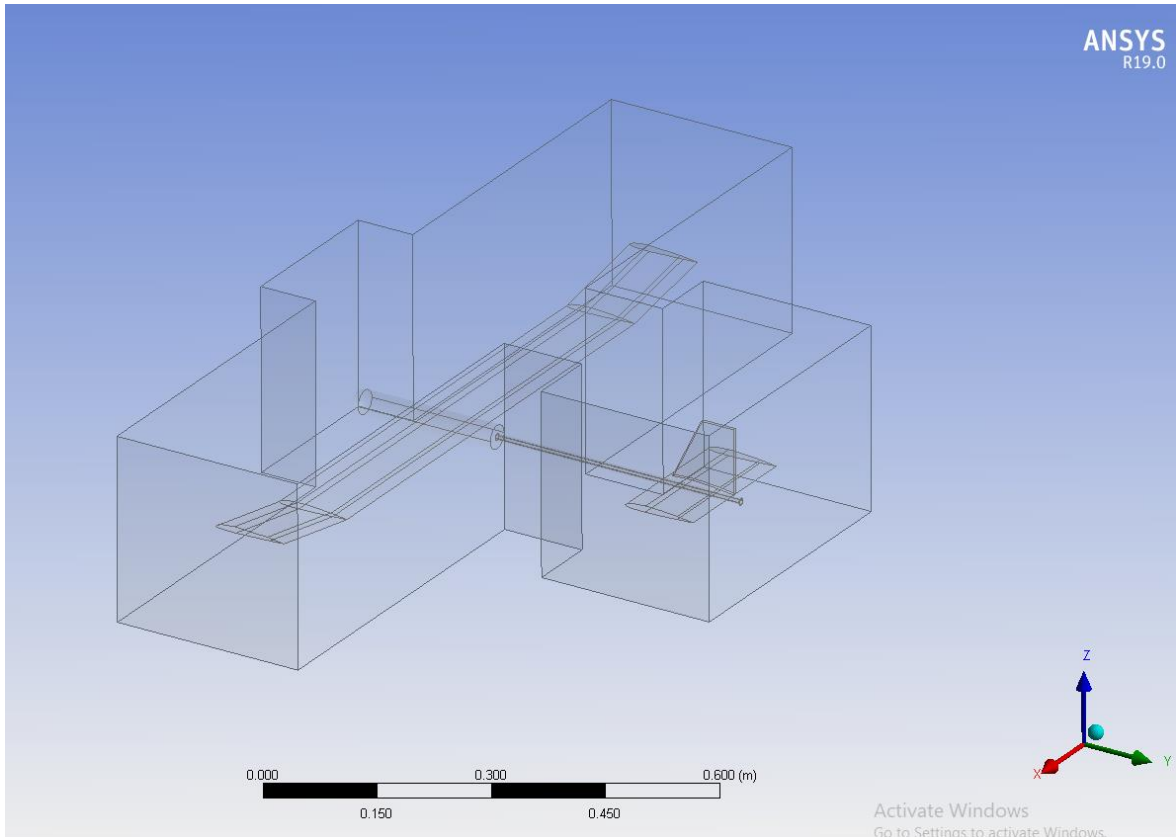


Figure 3.1: The geometry of glider UCC-14.

A three-dimensional glider is created in drawing software CatiaV5 and is imported into the ANSYS 19.2 workbench. The combination of hemisphere and cylindrical domain is set up for the 3-dimensional glider simulation. The distance of the glider is $6L$ from the front inlet surface and $12L$ to the outlet surface. The outlet surface is extended from $10L$ to $12L$ where by the L is the length of the glider to prevent backflow pressure.

3.3 Grid Generation

The domain is divided into 4 faces to enable the edge sizing method can be applied. A vertical split line is formed at the quarter of the chord which is at the aerodynamic center to create finer grid at the critical area. Numerical simulation needs fine computational grid in

low Reynolds number flows (Ma et al., 2015). The number of element for the mesh is 115000 for 2-dimensional analysis of airfoil.

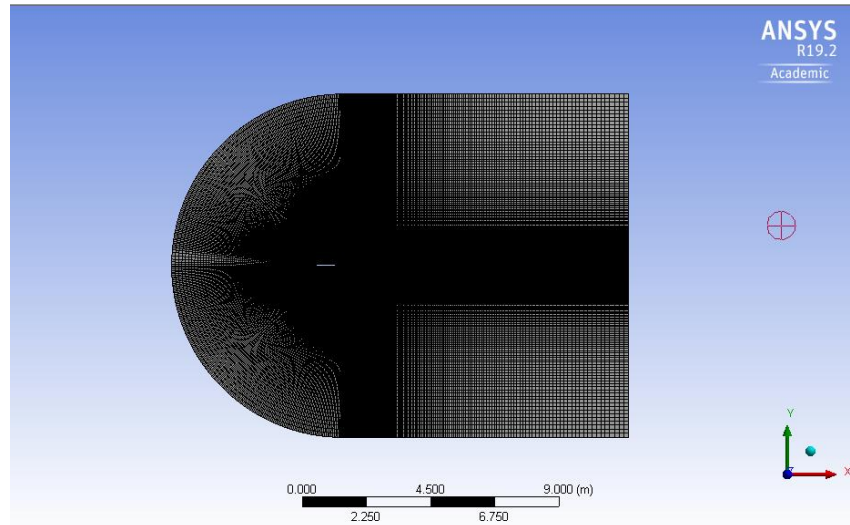


Figure 3.2: The t-type meshing with 4 faces.

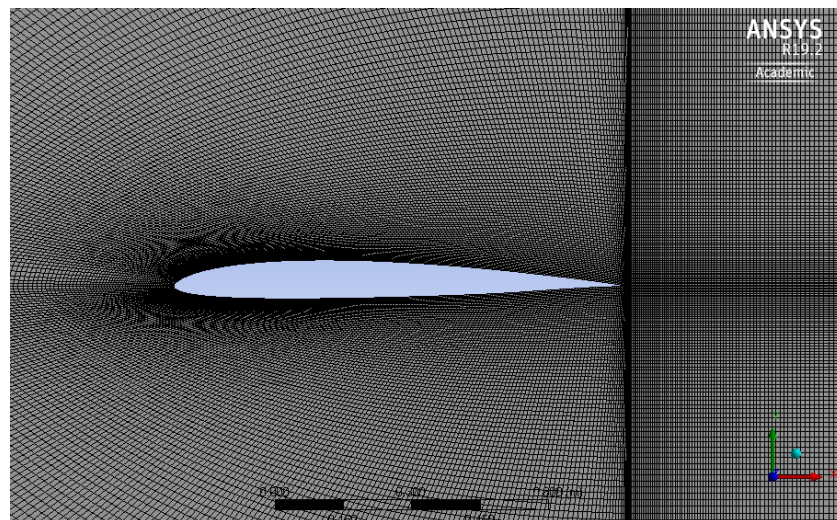


Figure 3.3: Meshing focusing near the airfoil area.

All the edges in the geometry is divided into a number of division to produce structured mesh as shown in the Figure 8. The structured grid is more preferable than unstructured grid

since it can avoid the divergence caused by rough grid (Ma et al., 2015) .T-type mesh is generated for this simulation.

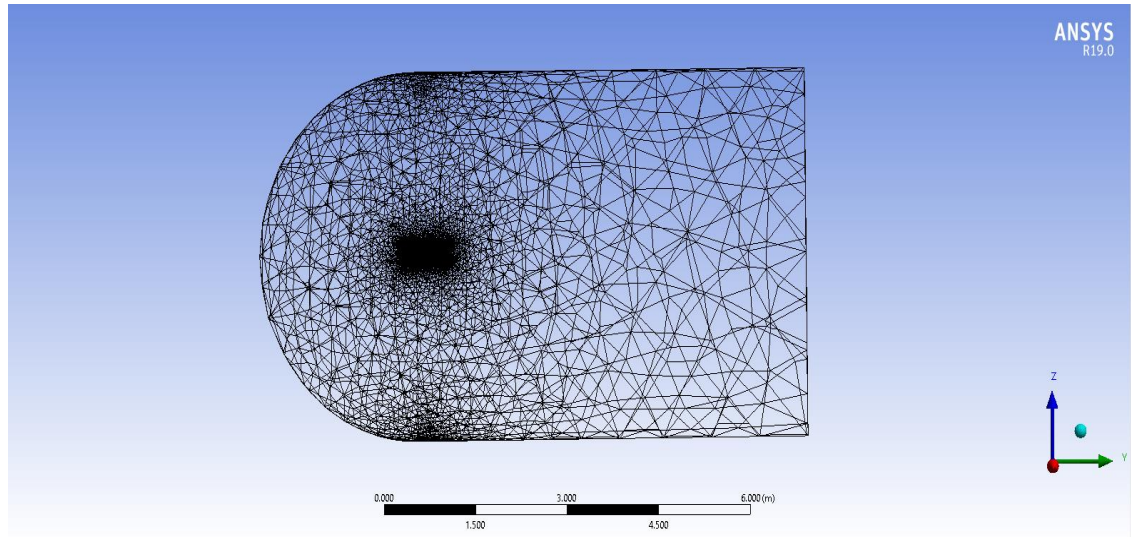


Figure 3.4: Grid generation for 3D glider in fluid domain.

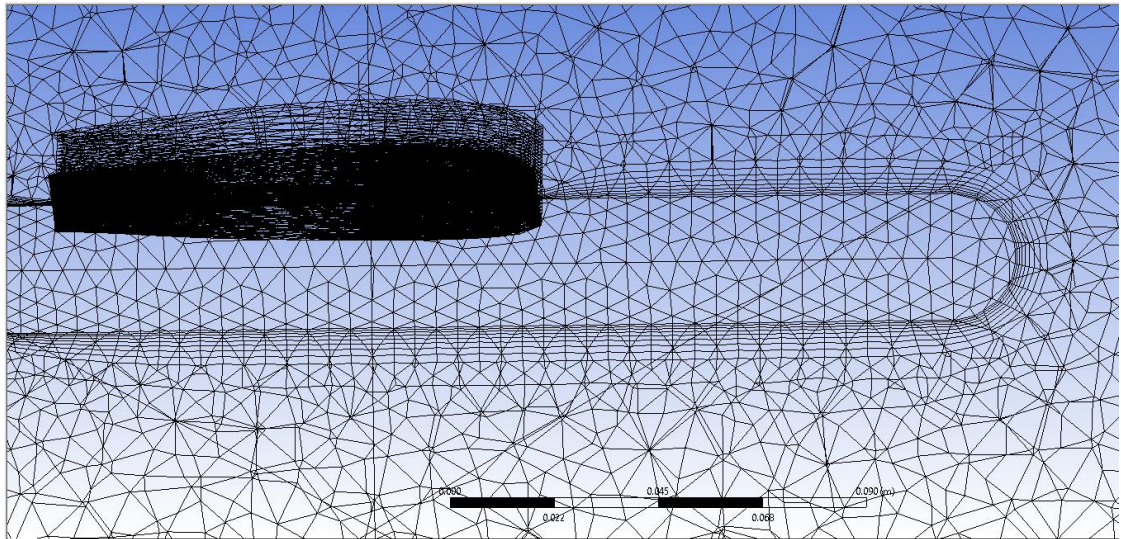


Figure 3.5: Meshing focusing on the inflation layer.

As for 3-dimensional analysis, a sufficient amount of face meshing has been applied to obtain the flow characteristic around the geometry surfaces. A very fine element are generated around the glider. Inflation layer method also has been applied around the curvy

edges of the geometry. Coarser elements are generated at the fluid domain. The total number of elements generated in this 3-dimensional case is 1024068.

In order to capture the laminar and transitional boundary layers correctly, the grid must have a y^+ of approximate to one (Langtry and Menter, 2005). y^+ is a non-dimensional distance which indicates the degree of fineness of grid in near-wall region.

3.4 Simulation Setup 2-Dimension

The simulation of all the 2-dimensional airfoils named RG-14, AG-37 and MH-32 are done in ANSYS Fluent 18.1. Laminar model is used to predict the flow characteristic. The fluid material is air with a constant density. The flow is dynamically identical as the velocity inside the domain is calculated corresponding to the wind tunnel Reynold's number which is 64000 with the chord length of the geometry drawn which is 1.0 m obtaining 0.8821 m/s. The upper and bottom wall as well as the semi-circle shape is set as the inlet velocity. The boundary line at the back of the airfoil is set to be the outlet pressure. The reference values computed from the inlet for the set up are as below:

Table 3.1: Input Parameter for the simulation setup of 2D.

Parameter	Value	Unit
Density	1.225	kg/m ³
Temperature	288.16	Kelvin
Velocity	0.8821	m/s
Viscosity	1.7894 e-05	kg/ms
Ratio of Specific Heat	1.4	

Both the governing equations and pressure have a precision of second order. In order to control the behavior of the flow, the under-relaxation factors are set as follow:

Table 3.2: Under relaxation factor for 2D analysis.

Parameter	Value	Unit
Pressure	0.17	N/A
Momentum	0.6	N/A

Relaxation factor is considered as under relaxed when the value is less than 1. Relaxation factor is a constant number and is used to alter the path of the iteration by multiplying it with the governing equations. The process of determining the best relaxation factor is quite challenging because it is only possible by trial and error method. The setup is then undergone hybrid initialization. The default under-relaxation factor set by ANSYS Fluent is 0.3 for pressure while 0.7 for momentum. The value should be reduced if the solution is observed to be instable or diverging. The solution is calculated for 10,000 iterations. The convergence criteria are absolute and unlimited to allow the residual to converge as much over time.

3.5 Simulation Setup for 3-Dimension

The simulation of the 3-dimensional model for UCC-14 glider (RG-14) is done in ANSYS Fluent 18.1. Laminar model is used to predict the flow characteristic. The fluid material is air with a constant density. The velocity set for 3D is calculated based on Reynold's number 64000 however this time corresponding to the total length of the glider which is 0.6 m obtaining 1.47 m/s. The domain wall around the glider is set as the inlet velocity. The surface at the back of the glider is set to be the outlet pressure. The reference values computed from the inlet for the set up are as below:

Table 3.3: Input Parameter for the simulation setup of 3D.

Parameter	Value	Unit
Density	1.225	kg/m ³
Temperature	288.16	Kelvin
Velocity	1.47	m/s
Viscosity	1.7894 e-05	kg/ms
Ratio of Specific Heat	1.4	

Both the governing equations and pressure have a precision of second order. In order to control the behavior of the flow, the under-relaxation factors are set as follow:

Table 3.4: Under relaxation factor for 3D analysis.

Parameter	Value	Unit
Pressure	0.1	N/A
Momentum	0.4	N/A

The setup is then undergone hybrid initialization. The solution is calculated for 10,000 iterations. The convergence criteria are absolute and unlimited to allow the residual to converge as much over time.

CHAPTER 4

RESULTS AND DISCUSSION

4.1 Introduction

This chapter explain, elaborated and discuss on the results obtain from the simulation and research done for this project.

4.2 Grid Independence Test

Grid independence test have been carried out in 2-Dimesional case (airfoil) to determine the best grid to be further use in the simulation setup. The grid that are tested consist of 85000, 100000, 115000 and 130000 number of elements. A graph has been plotted to compare the grids with the experimental data. The difference is shown clearly in Figure 13 with percentage difference for the 115000 element is 6.3% for Cl and 13% for Cd.

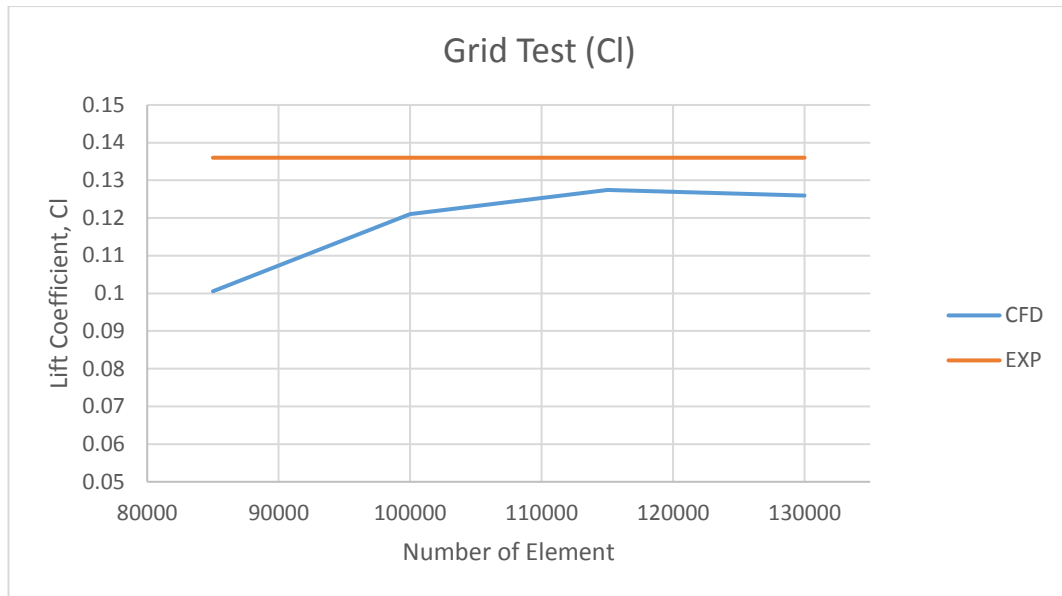


Figure 4.1: Comparison of different grids used in ANSYS with the experimental value of lift coefficient C_l .

Grid independence test is carried out at 0.93° angle of attack with Reynold's number of 60 400 using RG14 airfoil. The grid with 115000 number of elements is determined as the most suitable grid for the airfoil aerodynamic analysis. The grids between 100000 to 130000 is has reach stability which it does not make a huge difference to the result.

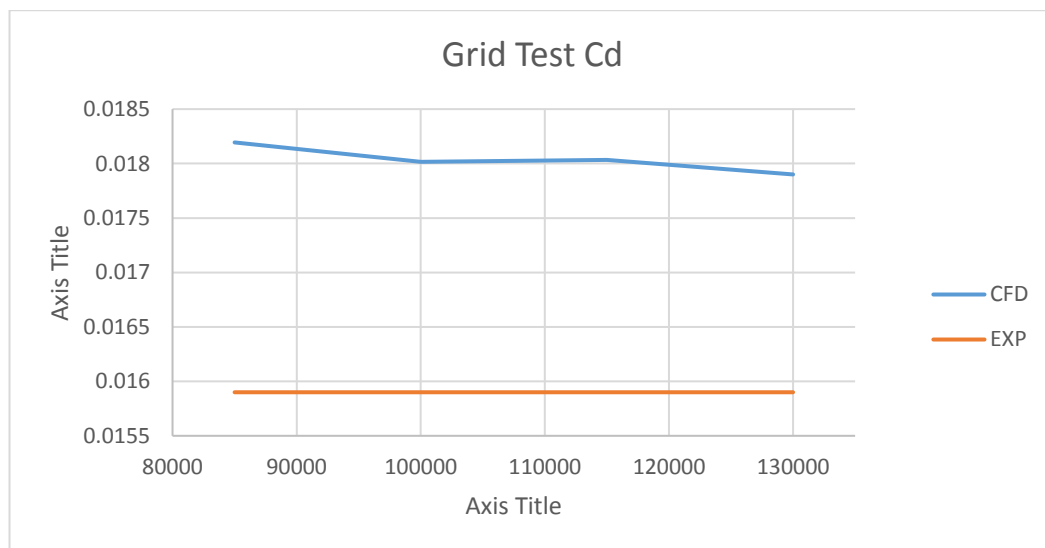


Figure 4.2: Comparison of different grids used in ANSYS with the experimental value of drag coefficient C_d .

The difference between the simulation data and the wind tunnel data is decreasing as the grids is refined to a higher number of elements. Hence, the accuracy of the results obtain from the simulation is higher and reliable than a coarser grid. Further refinement of the meshing is unnecessary because it will only increase the calculation and computational time rather than increasing the accuracy and efficiency of the results.

4.3 Result Validations

A set of wind tunnel experimental data is obtained from the '*Summary of Low-Speed Airfoil Data*' for RG14 airfoil. A setup in ANSYS Fluent is set to ensure the simulation result match the best with the wind tunnel data to validate its reliability and accuracy of the simulation setup. The flow condition is set to be dynamically identical with the same Reynold's number of 64 000. The simulation setup was able to reach convergence up to 1.0e-5.

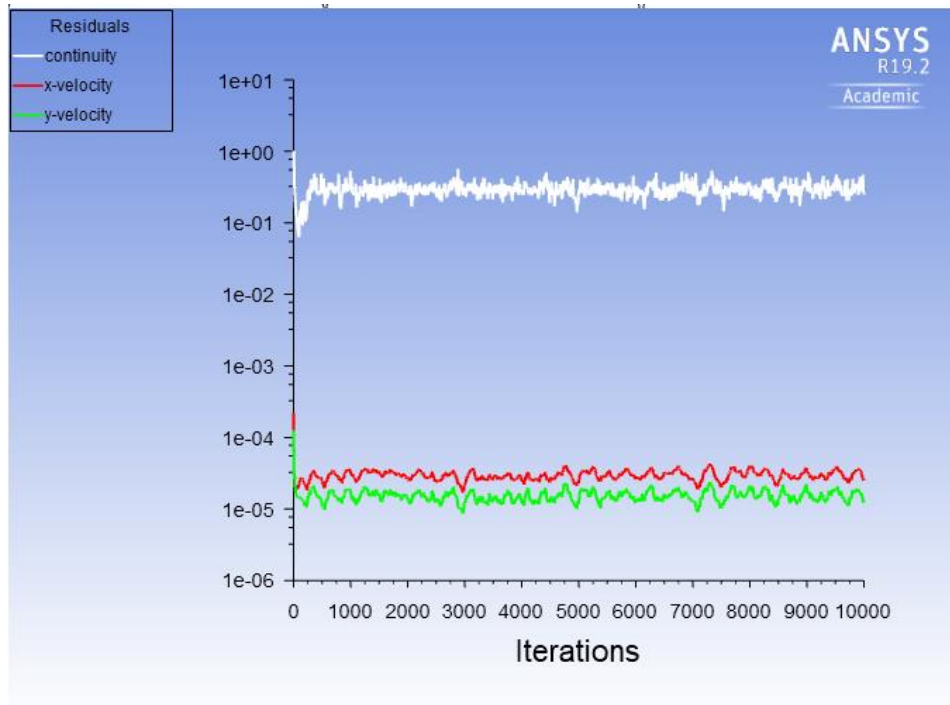


Figure 4.3: Residual plot showing the convergence of the solution.

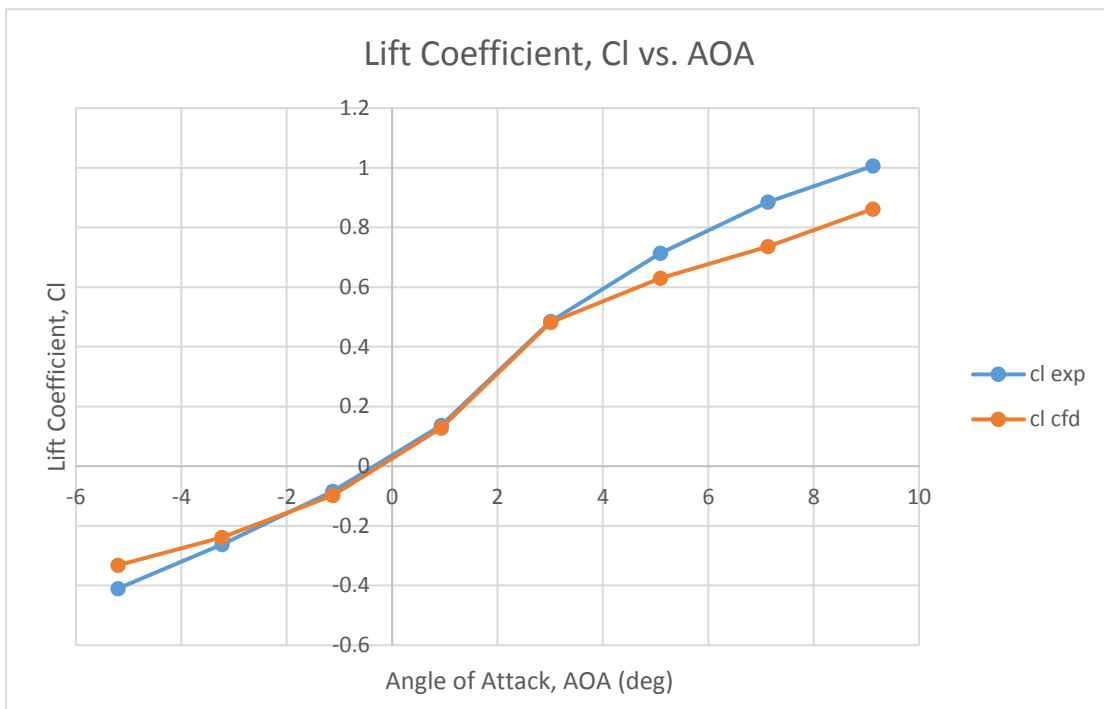


Figure 4.4: Graph of lift coefficient against the angle of attack for RG14 airfoil with experimental and computational data.

Based on the Figure 16 above, it can be seen that the lift coefficient from the computational calculations at the angle of attack of -3.0° to 3° almost overlapping each other with the experimental data. This shows that the gap value of the lift coefficients are very small. However, the lift coefficient plot started to deviate as the angle of attack is increased and decreasing away from zero degree angle of attack. Nevertheless, the percentage difference between the two plots is maintained at below 15%.

The explanation can be further discussed based on the velocity contour plot for RG14 provided in Table 9. A small flow circulation can be observed at the trailing edge of the airfoil. The flow circulation causes separation of boundary layer hence reducing the lift due to the disturbance to the pressure.

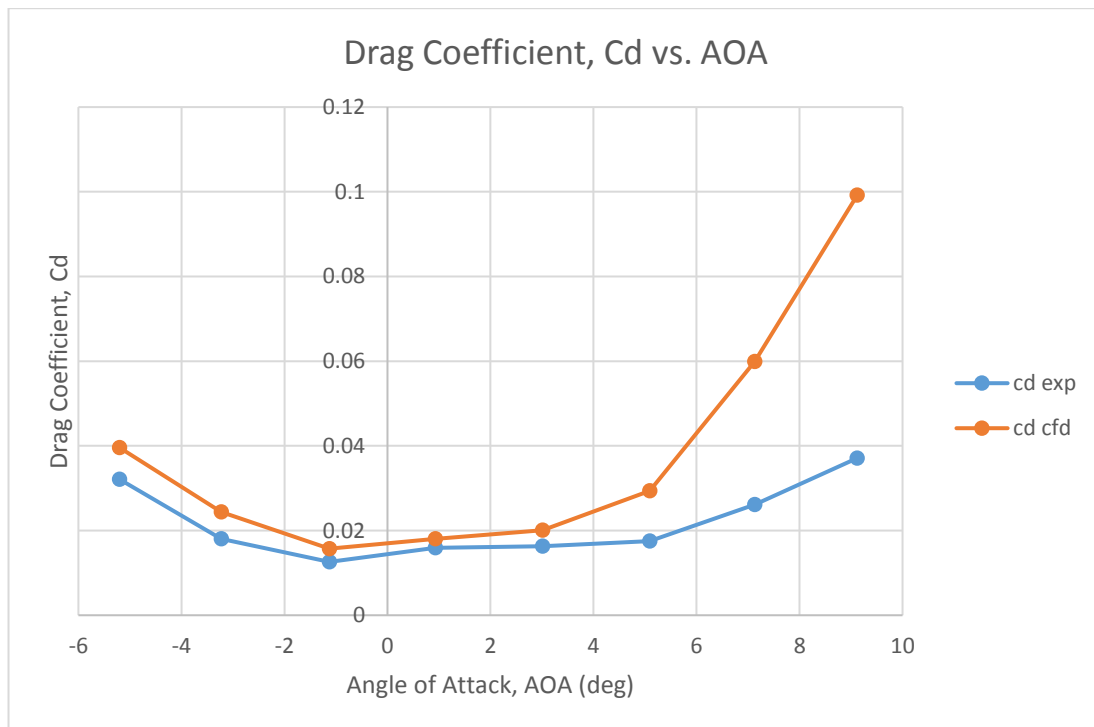


Figure 4.5: Graph of drag coefficient against the angle of attack for RG14 airfoil with experimental and computational data.